

# The WHaD diagram: Classifying the ionizing source with one single emission line

S. F. Sánchez<sup>1</sup>, A. Z. Lugo-Aranda<sup>1</sup>, J. Sánchez Almeida<sup>2,4</sup>, J. K. Barrera-Ballesteros<sup>1</sup>, O. Gonzalez-Martín<sup>3</sup>,  
S. Salim<sup>5</sup>, and C. J. Agostino<sup>5</sup>

<sup>1</sup> Instituto de Astronomía, Universidad Nacional Autónoma de México, A.P. 70-264, 04510, México, CDMX

<sup>2</sup> Instituto de Astrofísica de Canarias, La Laguna, Tenerife, E-38200, Spain

<sup>3</sup> Instituto de Radioastronomía and Astrofísica (IRyA-UNAM), 3-72 (Xangari), 8701, Morelia, Mexico

<sup>4</sup> Departamento de Astrofísica, Universidad de La Laguna, Spain

<sup>5</sup> Department of Astronomy, Indiana University, Bloomington, IN 47405, USA

Received —, 2023; accepted —, 2023

## ABSTRACT

**Context.** The usual approach to classify the ionizing source using optical spectroscopy is based on the use of diagnostic diagrams that compares the relative strength of pairs of collisional metallic lines (e.g., [O III] and [N II]) with respect to recombination hydrogen lines (e.g., H $\beta$  and H $\alpha$ ). Despite of being accepted as the standard procedure, it present known problems, including confusion regimes and/or limitations related to the required signal-to-noise of the involved emission lines. These problems affect not only our intrinsic understanding of inter-stellar medium and its poroperties, but also fundamental galaxy properties, such as the star-formation rate and the oxygen abundance, and key questions just as the fraction of active galactic nuclei, among several others

**Aims.** We attempt to minimize the problems introduced by the use of these diagrams, in particular their implementation when the available information is limited, either because not all lines are available or the do not have the required signal-to-noise.

**Methods.** We explore the existing alternatives in the literature to minimize the confusion among different ionizing sources and proposed a new simple diagram that uses the equivalent width and the velocity dispersion from one single emission line, H $\alpha$ , to classify the ionizing sources.

**Results.** We use aperture limited and spatial resolved spectroscopic data in the nearby Universe ( $z \sim 0.01$ ) to demonstrate that the new diagram, that we called WHaD, segregates the different ionizing sources in a more efficient way that previously adopted procedures. A new set of regions are defined in this diagram to select between different ionizing sources.

**Conclusions.** The new proposed diagram is well placed to determine the ionizing source when only H $\alpha$  is available, or when the signal-to-noise of the emission lines are too low to obtain reliable fluxes for the weakest emission lines involved in the classical diagnostic diagrams (e.g., H $\beta$ ).

**Key words.** ISM: general – Galaxies: ISM – Galaxies: active – Galaxies: star formation

## 1. Introduction

Understanding of which sources ionize the interstellar medium (ISM) in galaxies is of a paramount importance for the exploration not only of the properties of the ISM itself, but also for a correct evaluation of fundamental parameters, such as the star-formation rate or the metal abundance, that trace the current stage and past evolution of these objects (e.g., Kewley et al. 2019; Sánchez et al. 2021a, for recent reviews on the topic). Classically the dominant ionizing source, both galaxy wide or in a region within a galaxy, has been determined using the so-called diagnostic diagrams when using optical spectroscopy. These diagrams compare the distributions of different ionizing sources for a set of pairs of line ratios between collisionally excited emission lines (e.g., [O III]5007 and [N II]6584) and the nearest (in wavelength) hydrogen recombination line (e.g. H $\beta$  and H $\alpha$ ) (e.g. Baldwin et al. 1981; Osterbrock 1989; Veilleux et al. 2001).

The most frequently used of those diagrams, usually known as the BPT diagram (BPT Baldwin et al. 1981, see, Fig. 1, left panel), compares the distribution of the logarithm of the [O III]/H $\beta$  line ratio (O3) as a function of the logarithm of the [N II]/H $\alpha$  one (N2). In this diagram the ionization due to young-massive OB stars, those born in recent star-formation episodes,

follows a well defined arc-shape, with metal-rich ionizing stars at the bottom-right end of that arc and metal-poor ones at the top-left extreme. This arc is the result of the limited range of shapes of ionizing spectra for this kind of sources (being just a certain stellar type modulated by its metal content). On the contrary, ionizing sources with harder UV-spectra produce different line ratios, that could be in principal above the loci traced by OB-stars (Osterbrock 1989). Based on this physical principle, different demarcation lines have been proposed to classify the ionizing source. Among them, the most frequently used ones are those proposed by Kauffmann et al. (2003) and Kewley et al. (2001) to distinguish between ionization related to recent star-formation (SF) processes and those related to active galactic nuclei (AGN). Despite the fact that they have a very different origin and they are based on different assumptions (read Sec.4 in Sánchez et al. 2021a, for a detailed discussion on the topic), they are frequently used in combination to define three regimes in the O3-N2 plane, associated with three ionizing sources: (i) SF, below the Kauffmann et al. (2003) demarcation line, (ii) AGNs, above the Kewley et al. (2001) one, and (iii) mixed/intermediate, for values within both lines<sup>1</sup>.

<sup>1</sup> The list of references using this scheme is too large to cite them here

This approach is often far too simplistic and strongly biased by the overwhelming number of explorations using single aperture spectroscopic surveys (e.g., SDSS or GAMA York et al. 2000; Driver et al. 2009). First, the so-called intermediate regime could be populated by ionization purely related to a recent SF event, in particular in the presence of super-nova remnants (e.g. Cid Fernandes et al. 2021), or by ionization due to low-metallicity AGNs. This is indeed confirmed when exploring the location of X-ray selected AGNs in this diagram (X-AGNs, e.g., Agostino & Salim 2019; Osorio-Clavijo et al. 2023; Agostino et al. 2023) Thus, the concept of intermediate/mixed region is often misleading, as least in general, despite of the fact that this regime could indeed be populated by the mix of SF and harder ionization sources (Davies et al. 2016; Lacerda et al. 2018).

Finally, it is well known that other ionizing sources can mimic the line ratios usually associated to just AGNs when using this classification scheme. For instance, shocks presents a wide variety of line ratios depending on the properties of the ionized gas, the strength of the magnetic field and the velocity of the shock. High-velocity ones, those associated with galaxy-scale outflows (e.g. López-Cobá et al. 2020), have line ratios similar to those observed in strong AGNs (e.g. Veilleux et al. 2001). On the contrary, low-velocity ones, observed for instance in certain elliptical galaxies, present much lower line ratios (e.g. Dopita et al. 1996). Another key ionizing source in this kind of galaxies, and in non-SF retired galaxies in general (RG, Stasińska et al. 2008), or retired regions within galaxies (e.g. Singh et al. 2013; Belfiore et al. 2017; Lacerda et al. 2018), is the one produced by Hot evolved and post-AGB stars (Binette et al. 1994). The ionization by this stars produces weaker emission lines than those due to SF or AGNs (and shocks in many cases). However their line ratios cover a wide range of values, being as low as the values usually associated with SF or as high as the those classically assigned to AGNs (Sánchez 2020). We will refer to this ionization as RG along this article .

The distribution in the O3-N2 BPT diagram of both shocks and post-AGB ionization is very similar (e.g. Sánchez et al. 2021a). They cover the regime from the bottom-end of the SF distribution expanding towards larger values of both line ratios until reaching the same regime covered strong AGNs. They can also cover the same area known as low-ionization nuclear emission region (LINER Heckman 1987), that nowadays is not consider to be produced by low-luminosity AGNs in all the cases. Therefore, the line ratios adopted by the traditional BPT are not sufficient to separate between certain ionizing sources. To circumvent this problem, there have been proposed different strategies. For instance, Cid Fernandes et al. (2010) introduced the WHaN diagram, using the equivalent-width of  $H\alpha$ ,  $EW(H\alpha)$  (or  $WH\alpha$ ), a tracer of the relative intensity of the emission lines with respect to the underlying continuum, and the N2 ratio, as a tracer of the hardness of the ionization. In this diagram SF and AGNs are consider to have large values of  $EW(H\alpha)$ , with the former having lower values of N2 that the later. Regions ionized by hot evolved stars, present low values of  $EW(H\alpha)$  ( $<3\text{\AA}$ ), irrespectively of the N2 value. Based on a similar reasoning, Sánchez et al. (2014) proposed to combine the O3-N2 BPT diagram with the  $EW(H\alpha)$  to clean the SF regime from the contamination by low-N2 RG sources. Later Sánchez et al. (2018) generalized this idea, introducing the BPT+WHa diagram, in which the ionization is classified using both the BPT diagram and the  $EW(H\alpha)$  for all the considered ionizing sources.

The use of  $EW(H\alpha)$  helps to distinguish between RG and both SF and AGNs where they overlap in the BPT diagram. However,

it does not completely solve the problem of identifying the dominant ionizing source. For instance, in the case of shocks, both the location in the BPT diagram and the value of the  $EW(H\alpha)$  could be similar to that observed for AGNs (and SF in some cases). A possible solution is to explore the shape of the ionized structure, what it is only possible when spatial resolved spectroscopic data is available (e.g. Jarvis 1990; López-Cobá et al. 2017, 2019). An alternative strategy is to introduce the asymmetries in the emission lines and the velocity dispersion as an additional parameter to distinguish between different ionizing sources, or a combination of those kinematics parameters with the BPT, the location within the galaxy and/or the galactocentric distance (D'Agostino et al. 2019; López-Cobá et al. 2020; Johnston et al. 2023).

The methods including velocity information are indeed physical motivated: (1) SF happens in disks, and it requires low velocity dispersions to be triggered; (2) RG is associated with hot-evolves stars, that in general are found in bulges or thick disks, i.e., they are associated with regions of larger velocity dispersions than disks; (3) AGN ionization happens in the so called narrow-line regions <sup>2</sup>, that, despite of its name, presents much larger velocity dispersions than galaxy disks; and finally (4) shock ionization, by its very nature is associated with high-velocity dispersion clouds, due to the result of the compression and non uniform propagation of the galactic winds (shocks also produce multi-component and asymmetric emission lines). A recent exploration by Law et al. (2021) demonstrates that SF ionization is statistically associated with low velocity dispersion emission lines ( $\sigma_{\text{vel}} \sim 25\text{km s}^{-1}$ ), while harder ionizations are associated with a wide range of velocity dispersions, larger than  $>50\text{-}60\text{ km s}^{-1}$  in general. Indeed, the average distribution of the ionized gas velocity dispersions across the BPT diagram follows a similar, but oposite, pattern of that described by the  $EW(H\alpha)$  (e.g. Lacerda et al. 2018; Sánchez et al. 2021b, 2022).

Often the methods described above are insufficient. Determining the nature of the ionization requires the use of additional information, such as the shape of the ionized structures, the fraction of young stellar populations, the location within the galaxy and the galactocentric distance (e.g. D'Agostino et al. 2019; López-Cobá et al. 2020; Espinosa-Ponce et al. 2020; Sánchez et al. 2021a; Johnston 2022). The more additional parameters are used the more complicated is to observe all of them simultaneously with the required signal-to-noise to provide reliable classifications. Diagnostic diagrams based on line ratios require the simultaneous determination of the flux of four emission lines, not all of them of the same relative intensity (and signal-to-noise). For instance, in the case of the O3-N2 diagram it is often the case that  $H\beta$  is the limiting parameter. Ionizing sources that generate intrinsically weak emission lines, such as post-AGB/hot evolved stars, produce  $H\alpha$  fluxes barely detected with the current spectroscopic galaxy surveys in many cases. In those cases  $H\beta$ ,  $\sim 3$  times weaker, remains frequently undetected. A similar situation may happens in the presence of strong dust attenuation, like in the case of Ultra-Luminous Infrared galaxies, despite of the intrinsic luminosity of the ionized gas emission. As expected the situation becomes more complicated when more parameters are introduced. So, the seek for a more accurate classification is often hampered by the precision at which the involved parameters could be estimated.

One additional problem of most classical diagnostic diagrams like the BPT is the use of lines appearing in several different spectral regions. Due to technical limitations or the design

<sup>2</sup> for type-II AGNs, as type-I are the more easy ones to be identified by their distinguish feature of having broad Balmer lines

of the spectrograph, the lines cannot be observed simultaneously in a single setup (e.g., MEGARA Gil de Paz et al. 2018) or even with a single spectrograph (MUSE Bacon et al. 2010, and the need for BlueMUSE). These problems disappear if there were diagnostics based on a single line.

Motivated by the limitations of the currently adopted procedures to classify the ionizing source, and based on the most recent explorations that consider both the  $EW(H\alpha)$  and  $\sigma_{\text{vel}}$  as key parameters in this regards, we present here a single emission line diagnostic diagram that uses only those two parameters (the WHaD hereafter). We demonstrate that this diagram determines the nature of the ionizing source as well as the combination of the BPT diagram with the  $EW(H\alpha)$ , with the advantage of using just one single line and two parameters. We illustrate its use by comparing the spatial resolved classification of the ionizing source provided by the WHaD diagram with that provided by the BPT+WHa for a few archetypal galaxies, providing access to a similar comparison for a large galaxy sample.

The distribution of this article is as follows: the different datasets employed in this study are presented in Sec. 2, with both the analysis and results included in Sec. 3. Finally, the main conclusions are summarized in Sec. 4.

## 2. Data

We make use of the dataproducts provided by the `pyPipe3D` pipeline (Lacerda et al. 2022) for the integral field spectroscopy (IFS) data provided by the eCALIFA (extended Calar Alto Legacy Integral Field Area) survey (Sánchez et al. 2012, , Sanchez et al., submitted), and the final distribution of the MaNGA surveys (Mapping Nearby Galaxies at APO Bundy et al. 2015). Both surveys have been extensively described in the literature, in particular in the articles describing their most recent and final data releases (Sánchez et al. 2016a; Abdurro'uf et al. 2021) and Sánchez et al. (submitted), with a comparison between them included in a recent review on the topic of IFS galaxy surveys (Sánchez 2020).

To avoid repetitions we will not include a throughfull description of those surveys in here. For the purposes of the current exploration, we should highlight that: (i) both surveys observe a representative sample of galaxies in the nearby universe ( $z_{\text{CALIFA}} \sim 0.015$ ,  $z_{\text{MaNGA}} \sim 0.045$ ), covering a wide range of galaxy types and stellar masses, being complete above  $M_{\star} \sim 10^9 M_{\odot}$ , once applied the proper volume correction; (ii) the sample of galaxies is  $\sim 10$  times larger in the case of MaNGA ( $\sim 9000$  objects with good quality data) with respect to the sample covered by eCALIFA (895 objects), but the field-of-view of the IFS data ( $74''$  vs.  $19\text{--}32''$ ), the spatial coverage ( $2.5 R_e$  vs.  $1.5\text{--}2.5 R_e$ ), sampling and physical resolution ( $\sim 0.3$  kpc vs  $\sim 2$  kpc) is better/larger in the case of eCALIFA (in average); (iii) the spectral range (resolution) of the MaNGA data is  $\sim 2$  times larger (better) than that of eCALIFA,  $R \sim 2000$  vs  $\sim 850$  respectively. Nevertheless, in both cases is good enough for the purposes of this study; and finally (iv) both surveys cover the emission lines of interest for the current exploration ( $H\beta$ ,  $[O\text{III}]$ ,  $H\alpha$  and  $[N\text{II}]$ ), with enough signal-to-noise to measure the flux intensities, velocity dispersion and equivalent widths for the vast majority of the observed objects.

`pyPipe3D` is an automatic pipeline that performs a spectral decomposition of the stellar continuum and the ionized gas emission lines based on the stellar synthesis technique, assuming a particular template of single stellar populations (Sánchez et al. 2016b; Lacerda et al. 2022). This pipeline has been extensively used to study IFS data from different datasets, in-

cluding CALIFA (e.g. Cano-Díaz et al. 2016; Espinosa-Ponce et al. 2020), MaNGA (e.g. Ibarra-Medel et al. 2016; Barrera-Ballesteros et al. 2018; Sánchez et al. 2019a; Bluck et al. 2019; Sánchez-Menguiano et al. 2019), SAMI (e.g. Sánchez et al. 2019b), and AMUSING++ (Sánchez-Menguiano et al. 2018; López-Cobá et al. 2020). In addition, it has been tested using mock datasets based on hydrodynamical simulations (Guidi et al. 2018; Ibarra-Medel et al. 2019; Sarmiento et al. 2022). To avoid unnecessary repetition we do not include a description of the `pyPipe3D` either.

For the purpose, of the current exploration it is just relevant to know that for each analyzed datacube `pyPipe3D` provides the spatial distribution of a set of physical and observational parameters derived for both the stellar population and the ionized gas. In this study we make use of the spatial distributions of (i) the flux of the emission lines involved in the O3-N2 BPT diagram, (ii) the  $H\alpha$  velocity dispersion (corrected by instrumental resolution), and (iv) the  $EW(H\alpha)$ , all of them recovered based on the non-parametric moment analysis performed by this pipeline on the pure gas datacubes (i.e., the datacube once subtracted the best model spectra for the stellar component). All these dataproducts are publicly available distributed by Sánchez et al. (submitted) and Sánchez et al. (2022), as part of the corresponding eCALIFA and MaNGA data releases. It was also distributed the average value of each of these parameters at both the effective radius ( $R_e$ ) and in the central region of each galaxy ( $1.5''$  diameter and  $2.5''$  diameter for eCALIFA and MaNGA, respectively).

In addition, we make use of the results by Osorio-Clavijo et al. (2023), which have recently explored the X-ray properties of a sub-sample of the CALIFA galaxies, recovering  $\sim 40$  bona-fide AGNs. Finally, we use the O3 and N2 values of the sample of X-ray selected AGNs presented in Agostino & Salim (2019) for comparison purposes.

## 3. Analysis and Results

### 3.1. Classifying the ionization using the classical BPT diagram

As indicated in the introduction the procedure most frequently used to classify the ionization is the location of the O3 and N2 line ratios in the BPT diagram, combined, in some cases, with an additional parameter, for instance the  $EW(H\alpha)$ . Figure 1, left-panel, shows the distribution in this diagram of the different datasets described in the previous section, classified following the prescriptions outlined in Sánchez et al. (2021a), hereafter the BPT+WHa scheme: (1) RG, galaxies with  $EW(H\alpha)$  at  $R_e$  below  $3\text{\AA}$ , irrespectively of the location of the line ratios in the BPT diagram, not belonging to any of the other groups; (2) SF, galaxies with  $EW(H\alpha) > 6\text{\AA}$  and line ratios below the Kewley et al. (2001) demarcation line at  $R_e$ , and not belonging to any of the other groups; (3) O-AGNs, galaxies with a  $EW(H\alpha) > 6\text{\AA}$  and line ratios above the Kewley et al. (2001) in the central aperture. Note that for O-AGNs it is frequently distinguished between strong and weak AGNs adopting an  $EW(H\alpha) \sim 10\text{\AA}$  as the boundary between both categories. For AGNs, we selected the central aperture due to the dilution effect introduced by the ionized gas from the host galaxy (e.g. Sánchez et al. 2018; Osorio-Clavijo et al. 2023; Albán & Wylezalek 2023). Finally, we include the X-AGNs extracted from Osorio-Clavijo et al. (2023) and Agostino & Salim (2019); Agostino et al. (2023). Note that most objects are well classified using this scheme, with just a few objects without a well defined dominant ionizing source.

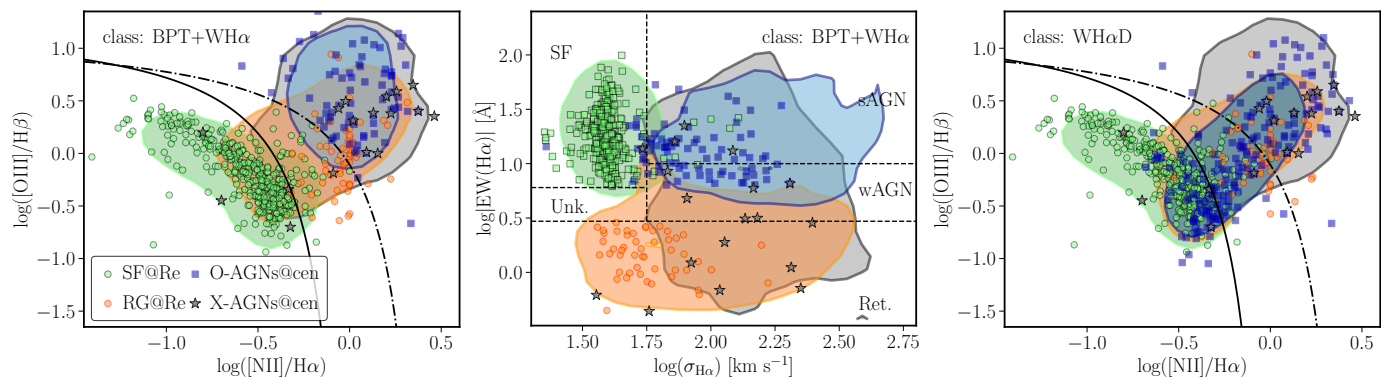


**Fig. 1.** *Left panel:* classical BPT diagram (Baldwin et al. 1981), showing the distribution of  $[\text{O III}]/\text{H}\beta$  line ratio as a function of  $[\text{N II}]/\text{H}\alpha$  ratio. It includes four sub-samples of objects whose ionization has been classified according to this diagram together with  $\text{EW}(\text{H}\alpha)$ , following Sánchez et al. (2021a): (i) star-forming galaxies (SF, green), (ii) retired galaxies (RG, orange), (iii) optically selected AGNs (O-AGNs, blue) and (iv) X-ray selected AGNs (X-AGNs, black stars). Solid symbols correspond to data extracted from the eCALIFA sample, with the X-AGNs being extracted from Osorio-Clavijo et al. (2023). The shaded regions correspond to data extracted from the MaNGA sample (SF, RG and O-AGNs) and from Agostino & Salim (2019) (X-AGNs), showing the area encircling 90% of the objects in each case. The region at which the ionization was measured is indicated in the legend: central aperture (cen) or at the effective radius (Re). Solid and dot-dashed lines correspond to the classical demarcation lines proposed by Kauffmann et al. (2003) and Kewley et al. (2001) to distinguish between the different ionizing sources. *Middle panel:* new proposed diagnostic diagram (WH $\alpha$ D) showing the distribution of the  $\text{EW}(\text{H}\alpha)$  (or WH $\alpha$ ) as a function of the  $\text{H}\alpha$  velocity dispersion for the same sub-samples of objects included in the previous panel, using the same nomenclature. It is clearly appreciated that the different ionizing sources are well separated in this new diagram. Dashed lines correspond to the proposed demarcation lines to separate between different dominant ionizing sources, with the corresponding sources indicated. *Right-panel:* distribution in the BPT diagram shown in the first panel of the eCALIFA (solid symbols) and MaNGA (shaded regions) galaxies classified according to the location of their ionization in the WH $\alpha$ D diagram, measured at the same two locations indicated for the values shown in the first panel. The location of the X-ray selected AGNs has been included for completeness.

By construction the SF galaxies are located where it is expected. They follow a clear arc-shaped distribution not only below the adopted demarcation line (Kewley et al. 2001), but in most of the cases below the more restrictive Kauffmann et al. (2003) one ( $\sim 92\%$  of the objects). A similar behavior is found for the O-AGNs, that by construction are located above the Kewley et al. (2001) curve. Thus, SF can be distinguished from O-AGNs using just the BPT diagram and the classical demarcation lines. However, the situation is not that simple when RG are included. It is clear that galaxies (and regions within them) with low  $\text{EW}(\text{H}\alpha)$  are distributed in the right-branch of the BPT diagram, covering a wide range of values. Some 17% of them are below the Kauffmann et al. (2003) curve,  $\sim 54\%$  in the intermediate region between that line and the Kewley et al. (2001) one, and  $\sim 28\%$  above that line. Thus, without introducing an additional parameter, in this case the  $\text{EW}(\text{H}\alpha)$ , it is not possible to distinguish between this ionizing source and SF or O-AGNs.

We should note that the current selection of O-AGNs does not guarantee that all AGNs are selected. It is well known that, in many instances, radio-galaxies do not present signatures of optical AGNs regarding their line ratios and/or flux intensities (e.g., Comerford et al. 2020, and references therein). Other *bona fide* AGNs, like those detected in X-rays, present emission lines in the optical which ratios are not above the demarcation lines adopted to select O-AGNs in many cases. We include in Fig. 1, left-panel, the distribution of the 424 X-ray selected AGNs by Agostino & Salim (2019) and Agostino et al. (2023) (X-AGNs hereafter), with the emission lines obtained from the SDSS spectroscopic data. It is clear that they are not restricted to the same regime usually adopted to select O-AGNs, covering a range of values more similar to the one observed for RG. Indeed, in the case of this particular sample of X-AGNs, only 34% of them would be classified as O-AGNs, 28% as RGs and 20% as SF galaxies, using the BPT-WH $\alpha$  classification scheme (Sánchez

**Table 1.** Results of the 2D Kolmogorov-Smirnov test

Method	BPT+WH $\alpha$	WH $\alpha$ D
SF vs RG	0.752	0.953
SF vs O-AGNs	0.981	0.946
SF vs X-AGNs	0.877	0.961
RG vs O-AGNs	0.495	0.927
RG vs X-AGNs	0.311	0.578
O-AGNs vs. X-AGNs	0.261	0.426

et al. 2021a). This is usually interpreted as a dilution effect by the contamination of other ionizing sources, such as circumnuclear or host-galaxy star-formation, or obscuration of the optical emission. However, a similar behavior is observed in the distribution of the line ratios extracted from the central aperture ( $< 1\text{kpc}$ ) of the X-AGNs selected from the CALIFA sample itself studied by Osorio-Clavijo et al. (2023). In this case the fraction of objects classified as O-AGNs is even lower (17%), using the BPT-WH $\alpha$  scheme. Furthermore, Agostino et al. (2021) demonstrated that once subtracted the SF contribution to the integrated SDSS spectra of a sample of Seyfert galaxies a large number of them are still found below the Kauffmann et al. (2003) demarcation line. In summary, neither the BPT along nor its use combined with the  $\text{EW}(\text{H}\alpha)$  guarantee a clean separation of AGNs from other ionizing sources.

### 3.2. BPT-classified ionizing sources across the $\text{EW}(\text{H}\alpha)$ - $\sigma_{\text{H}\alpha}$ (WH $\alpha$ D) diagram

We explore now the ability to classify the ionizing source using just the  $\text{EW}(\text{H}\alpha)$ , that has been proved to be crucial to distinguish between RG and other ionizing sources, and the velocity

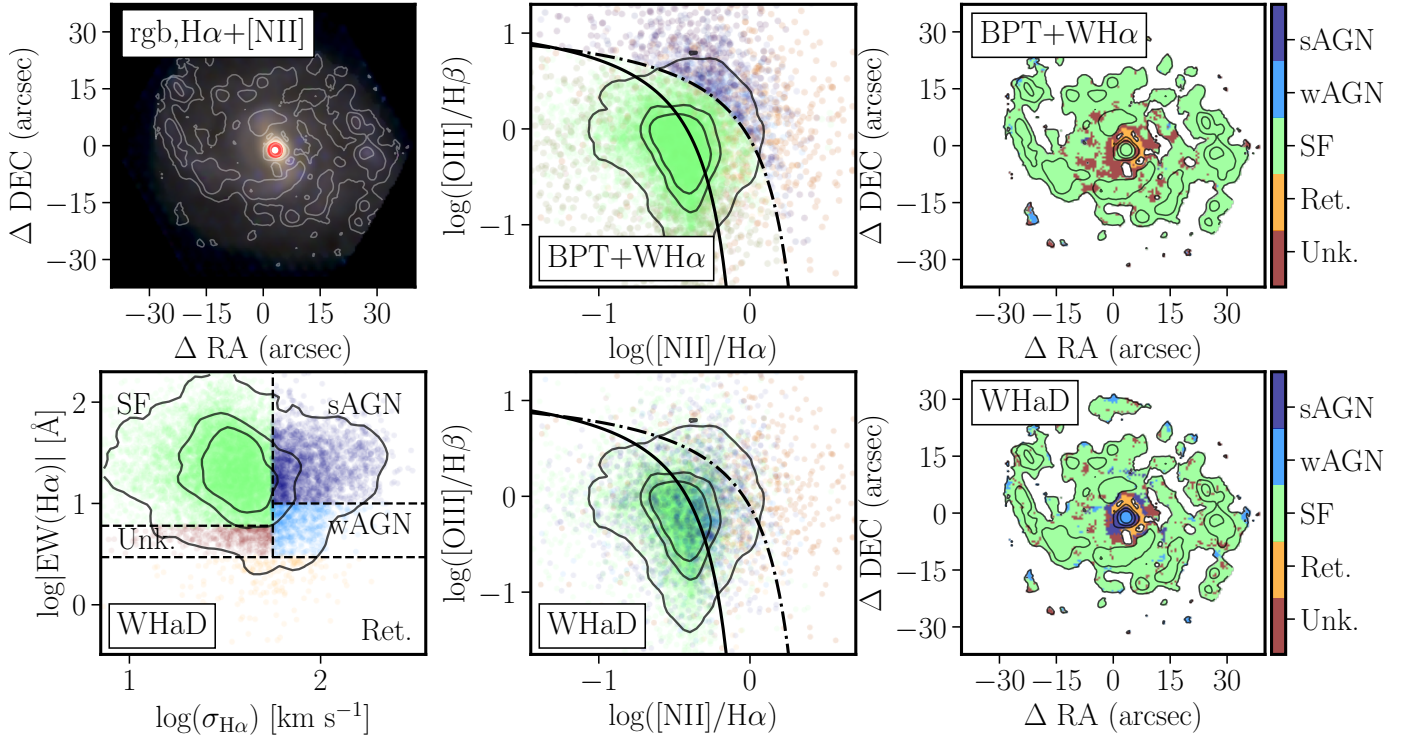


**Fig. 2.** *Top-left panel:* RGB-image created using the  $r$ -,  $g$ - and  $r$ -band images synthesized from the eCALIFA datacube of NGC 5947, together with a set of contours showing the  $H\alpha$ + $[NII]$  flux intensities, with the 1st contour corresponding to the mean value minus one standard deviation, and each successive contour following a multiplicative scale of five times that value. The red-circle indicates the central aperture adopted along this article (e.g., Fig. 1). *Top-middle panel:* classical diagnostic diagram showing the distribution of  $[OIII]/H\beta$  line ratio as a function of the  $[NII]/H\alpha$  ratio for each individual spaxel of the same cube shown in the top-left panel, color coded by nature of the ionization according to the classification based on location in this diagram together with the  $EW(H\alpha)$ , thus, the same selection criteria adopted in top-left panel of Fig. 1: SF in green, RG in orange and AGN-like ionization in blue. *Top-right panel:* spatial distribution of the ionized gas for those spaxels with  $H\alpha$  above the mean minus one standard deviation value, color coded by the classification shown in the middle panel (i.e., BPT+WH $\alpha$ ). Those spaxels with  $H\alpha$  flux with a signal-to-noise below 3 or any of the remaining emission lines involved in the BPT diagram below 1 are marked as unknown (dark-red color). Contours are the same already shown in the top-left panel. *Bottom-left panel:* distribution along the WHaD diagram,  $EW(H\alpha)$  vs.  $\sigma_{H\alpha}$ , for the individual spaxels of the same datacube shown in the previous panels, color coded according to the classification of the ionizing source based on the location within this diagram. *Bottom-middle panel:* diagnostic diagram similar to the one already shown in top-middle panel, with the individual spaxels color coded following the new classification based on the WHaD diagram (bottom-left panel). *Bottom-right panel:* spatial distribution of the ionized gas similar to that shown in the top-right panel, this time color-coded with the classification obtained using the WHaD diagram shown in the bottom-left. The similarities and differences between the two classification schemes are evident when comparing top- and bottom-right panels.

dispersion ( $\sigma_{vel}$ , following D’Agostino et al. 2019; López-Cobá et al. 2020; Law et al. 2021; Johnston 2022). Figure 1, central panel, show the distribution of the  $EW(H\alpha)$  as a function of  $\sigma_{H\alpha}$ , hereafter WHaD diagram, for the same dataset included in the BPT diagram (left-side diagram). It is clear that that three categories of ionizing sources selected using the BPT+WH $\alpha$  are located in three distinguishable regions. SF galaxies are all restricted to a narrow range of low velocity dispersions and high  $EW(H\alpha)$ . Indeed, as already noticed by Law et al. (2021), there is a very low number of SF galaxies with a velocity dispersion above  $>50 \text{ km s}^{-1}$  ( $\sim 2\%$ ), with most of them located in a regime  $\sim 25 \text{ km s}^{-1}$ . On the other hand, RG occupy the regime of low  $EW(H\alpha)$  by construction. In addition, they cover a wider range of velocity dispersions, from  $\sim 30 \text{ km s}^{-1}$  to  $\sim 300 \text{ km s}^{-1}$ , with an average value  $\sim 90 \text{ km s}^{-1}$  (slightly lower for eCALIFA than for MaNGA). Finally, the O-AGNs are limited to a regime of high  $EW(H\alpha)$  by construction, covering an even wider  $\sigma_{H\alpha}$  range, with larger values for MaNGA than for eCALIFA. Regarding the X-AGNs we do not have the required information to replicate the distribution shown in the BPT diagram for the Agostino & Salim (2019) dataset, however, the sample studied by Osorio-

Clavijo et al. (2023) distributed across the entire diagram, with a preference to larger velocity dispersions than the SF sample.

We quantify the ability to segregate the different ionizing sources using the WHaD diagram in comparison with the BPT one by performing a 2D Kolmogorov-Smirnov (KS) test (using the `NDTEST` python package). Table 1 lists the values of the KS statistics obtained by comparing the distributions of the different ionizing subsamples selected based on the BPT+WH $\alpha$  criteria applied to the MaNGA dataset (SF, RG and O-AGNs) in addition to the Agostino & Salim (2019) sample (X-AGNs) across the O3-N2 BPT and the WHaD diagrams. We adopted these subsamples as they are the ones with the largest number of objects (i.e., a better statistical coverage of the explored parameters). The result of this test indicates that the new diagram segregates the different subgroups in a more efficient way.

Based on the described distributions and the results of the KS-test, we define five regimes in the WHaD diagram. First, using same criteria introduced by Cid Fernandes et al. (2010) when introducing the WHaD diagram, and adopted in the BPT+WH $\alpha$  scheme, we classify as RG those sources with an  $EW(H\alpha) < 3 \text{ \AA}$ .

<sup>2</sup> <https://github.com/syrte/ndtest>

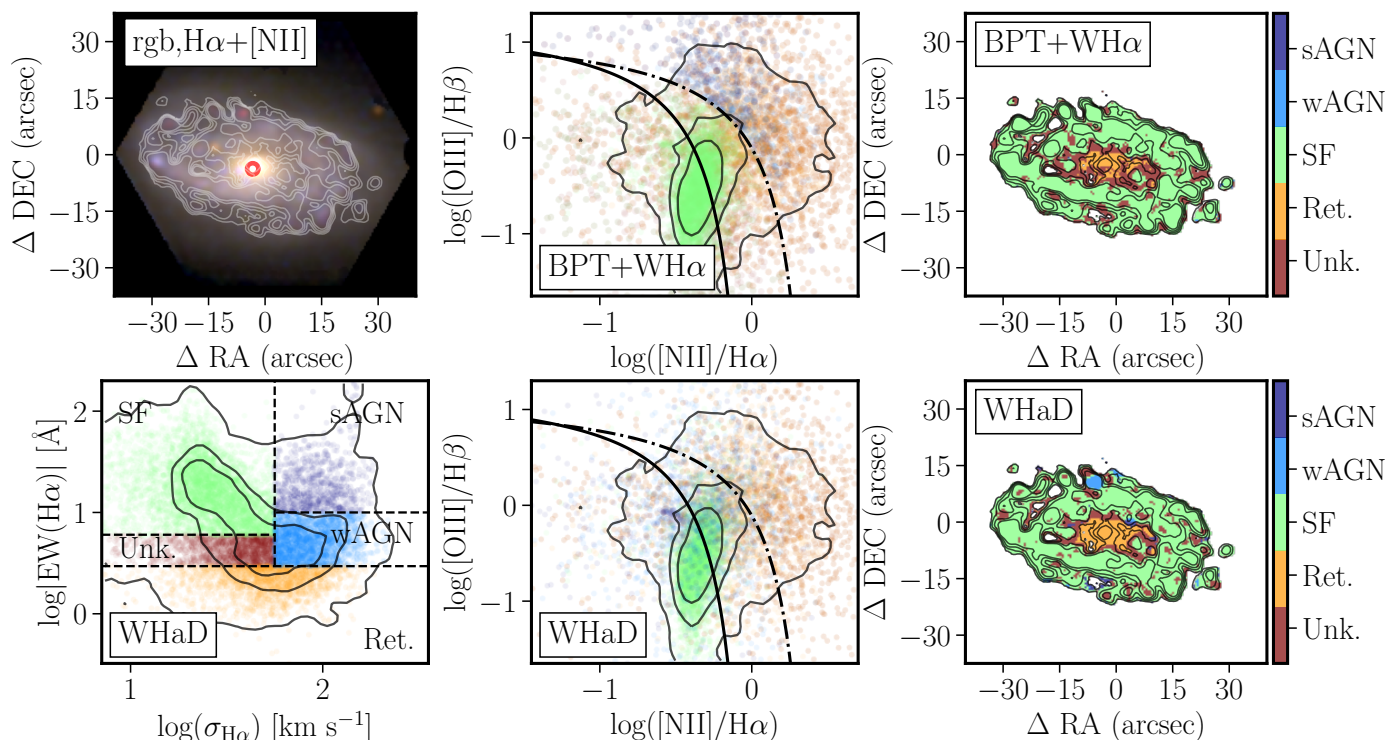


**Fig. 3.** Similar to Fig. 2, corresponding to the eCALIFA data of NGC 2906

Then we classify as SF those sources with a  $EW(H\alpha) > 6 \text{ \AA}$  (following Sánchez et al. 2014) and  $\sigma_{H\alpha} < 57 \text{ km s}^{-1}$ , a region that comprises 98% (90%) of the eCALIFA (MaNGA) previously selected SF galaxies. In addition, we define as O-AGNs those sources with a  $EW(H\alpha) > 3 \text{ \AA}$  and a  $\sigma_{H\alpha} > 57 \text{ km s}^{-1}$ , distinguishing between weak-AGNs (wAGN) and strong-AGNs based on the  $EW(H\alpha)$ , using  $10 \text{ \AA}$  as a boundary between both regimes. Based on these criteria 86% (95%) of the O-AGNs selected using the BPT+ $WH\alpha$  scheme would remain as O-AGNs, and 14% (1%) would be reassigned as SF in the case of the eCALIFA (MaNGA) sample. Note that the boundary in the velocity dispersion was empirically selected to maximize (minimize) the agreement (disagreement) between the classifications provided by the classical BPT diagram and the new proposed WHaD diagram for the optically selected SF and O-AGNs.

If we consider that the BPT- $WH\alpha$  scheme does actually reproduce the real distribution of ionizing sources, the new classification based on the WHaD diagram would be 100% reliable for the RG (as it is essentially the same scheme), between a 90-98% reliable for SF galaxies, and just a 86-95% reliable for O-AGNs. However, we should keep in mind that the initial scheme is based on some pre-conceptions, like the fact that AGNs should present strong emission lines produced by a hard ionization (i.e., high values of both O3 and N2). As indicated before this is not always the case. Figure 1, left- and central-panels, shows that bona-fide X-AGNs may present a wide range of O3-N2 line ratios and an equally wide range of  $EW(H\alpha)$  values. Regarding X-AGNs, we already established that only 17-34% of those studied by Osorio-Clavijo et al. (2023) and Agostino & Salim (2019) are classified as O-AGNs using the BPT+ $WH\alpha$  scheme. This fraction increases to a 50-53% when using the newly introduced WHaD classification procedure. This particularly relevant, as X-AGNs are the only sources for which the ionization source is fully determined. Based on these results, we should not consider that a

priori the BPT- $WH\alpha$  offers a better classification scheme than the currently proposed one.

### 3.3. Classifying the ionization using the WHaD diagram

Based on this exploration we re-classified the eCALIFA, MaNGA galaxies and the X-AGN samples studied in the previous sections using the new WHaD diagram and the boundaries proposed before. Figure 1, right-panel, shows the distribution along the O3-N2 BPT diagram based on this new classification, using the same nomenclature as the one adopted in the left- and central-panels. As a first result, we highlight that the distribution for RGs is the same. Regarding the SF galaxies, besides the increase in the number of galaxies (plus 8%), the distributions are very similar. Only  $\sim 1\%$  of the newly classified SF galaxies would be classified as AGNs using the BPT+ $WH\alpha$  scheme. The main difference is found for the O-AGNs, that now are not restricted to the upper-end of the right-branch in the BPT diagram. Indeed, they follow a distribution more similar to that of the RG or the X-AGNs in this diagram. About 27% (50%) of the eCALIFA (MaNGA) galaxies classified as O-AGNs with the new WHaD scheme would be SF based on the BPT+ $WH\alpha$  method. Although this could be due to a misclassification introduced by the new procedure, we consider more probable that we have disclosed a larger population of AGNs thanks to the new method.

As a final remark, we stress that the results for both datasets, eCALIFA and MaNGA, are remarkable similar despite of the reported differences between the two datasets, outlined in Sec. 2. The major differences are found in the fraction of previously selected O-AGNs (SF) that are not classified as SF (O-AGNs), in which both samples disagree by  $\sim 20\%$ . In this regard, we remind that both samples have different selection functions and so far we have not applied any correction for the selection function. Thus,

the reported differences could be just due to the different sample selections.

### 3.4. Spatial distribution of the ionizing sources using the WHaD diagram

In previous sections we describe how the dominant ionizing source is determined, for different galaxies (and apertures within them), using a rather classical/well-established approach (Sec. 3.1) in comparison with the new scheme proposed in this study (Sec. 3.2-3.3). As already indicated in the introduction, and discussed in several previous studies (e.g. Sánchez 2020; Sánchez et al. 2021a, and references therein), the ionization is a process that happens at scales smaller than the integrated galaxy scale discussed in the previous sections. Like in the case of the integrated or aperture limited spectra (e.g. Kauffmann et al. 2003), diagnostic diagrams and/or a combination of them with additional parameters is a well established procedure to identify the different ionizing sources that may be present in a galaxy when using spatial resolved spectroscopy data (e.g. Law et al. 2021; Johnston 2022; Sánchez et al. 2023, for citing just a few). To demonstrate that the WHaD diagram provides with a spatial resolved classification of the ionizing source as good or even better than the one provided by the BPT+WHa scheme, we have applied both methods to the spatial resolved dataproducts derived using `pyPipe3D` for the full IFS dataset provided by the last eCALIFA data release (Sanchez et al. 2023; Sánchez et al. 2023), already described in Sec. 2. We distribute the outcome of this analysis through the web<sup>3</sup>, describing here in detail the results derived for four cherry-peaked galaxies that illustrate the general behavior.

Figure 2 shows the comparison between the spatial resolved distribution of the ionizing sources identified based on the BPT+WHa scheme and the WHaD diagram for NGC 5947. This is a low inclination early spiral, with a morphology (SBbc) and stellar mass ( $\sim 10^{10.5} M_{\odot}$ ), very similar to that of the Milky-Way (indeed, it hosts a solar-neighborhood analog region too; Mejía-Narváez et al. 2022). Figure 2, top-left panel, shows an optical three-color image extracted from the datacube, that traces the light distribution from the stellar continuum. Contours trace the distribution the combined flux intensities of H $\alpha$  and [N II]. As expected, the regions with stronger ionized-gas emission trace the location of the spiral arms, although there is detectable ionized gas across most of the optical extension of the galaxy. The distribution across the [O III] vs. [N II] diagnostic diagram for the individual spaxels is included in the top-middle panel, color-coded according to the BPT+WHa classification scheme (Sec. 3.1), with the spatial distribution of the different ionizing sources shown in the top-right panel. In this particular implementation of the classification scheme, we considered that the ionizing source cannot be correctly identified if the S/N ratio of H $\alpha$  is lower than three, and below one for the remaining emission lines involved in this diagram. Note that for the identification of retired regions, this criteria could be relaxed, adopting just a cut in EW(H $\alpha$ ). As expected, due to the nature of this galaxy, most of the optical extension is dominated by ionization related to recent SF. Only a small annular circumnuclear region of  $\sim 5''$  present an ionization classified as retired (or unknown). Finally, based on this scheme the ionization in the central region ( $< 3''$ ) is classified as SF.

The distribution of spaxels along the WHaD and BPT diagrams for NGC 5947 are included in bottom-left and bottom-

central panels of Fig. 2, color coded according to the new classification scheme (Sec. 3.3), with the spatial distribution of the new classified ionizing sources shown in bottom-right panel. Despite of the fact that the distribution across the BPT diagram looks very different, the spatial distribution of the different ionizing sources is rather similar. Most of the spaxel are classified as SF, covering a similar region as the one covered by the previous classification, roughly corresponding to the disk of the galaxy. The annular region around the center is equally classified as retired (or unknown). However, contrary to the previous classification the ionization in the central region is classified as wAGN/sAGN. Based on the results discussed in previous sections we cannot conclude that this is a miss-classification, as up to  $\sim 20\%$  of bona-fide AGNs (e.g., X-AGNs) could present line ratios compatible with SF, even when the spectroscopic information is restricted to the central apertures (e.g. Agostino & Salim 2019; Osorio-Clavijo et al. 2023). On the other hand, we cannot neither exclude the possibility that this is a missclassification introduced by the new method too. . So far, the presence of an AGN has not been confirmed in NGC 5947 using non-optical observations.

Figure 3 presents similar plots for NGC 2906. This is a late type, almost face-on, spiral galaxy slightly less massive than NGC 5947 ( $M_{\star} \sim 10^{10} M_{\odot}$ ). Like in the previous case, the ionization is classified as SF for most of the regions, in particular, for those in the galaxy disk. However, contrary to the previous galaxy, all the ionization in the central regions ( $< 10''$ ) is classified as retired (or unknown). The two classification schemes (BPT+WHa and WHaD) provide very similar results. Thus, the spatial distributions of the ionizing sources included in top- and bottom-left panels of Fig. 3 are almost undistinguishable. However, when looking in detail, the WHaD scheme classifies as wAGN/sAGN a circular region region  $\sim 12''$  North and  $\sim 5''$  East from the center of the galaxy. On the contrary, based on the BPT+WHa method, the ionization at this location would be classified as SF. Like in the previous case we could consider that this is missclassification of the new method, as obviously an off-center AGN is unlikely. However, it is known that a supernova exploded in this galaxy at this exact location before the observing run (SN 2005ip, Lee et al. 2005), and where a supernovae remnant has been identified (SNR; Martínez-Rodríguez in prep.). We must recall that AGN ionization cannot be distinguished from other sources of ionization such as shocks or SNR based only in the exploration of the BPT diagram, and additional parameters have to be introduced (e.g., López-Cobá et al. 2020; Cid Fernandes et al. 2021, , and in the introduction). However, the WHaD diagram seems to pinpoint SNR that are well below the classical demarcation lines adopted to separate SF regions from other sources of ionization.

Motivated by the previous result we explore how the classifications based on the two methods compare in the presence of evident shock ionization. Figure 4 shows the same plots already included in Fig. 2 and 3 for the edge-on spiral galaxy NGC 6286. This is a luminous infrared galaxy (Howell et al. 2010) that presents a well studied galactic outflow (e.g. López-Cobá et al. 2019, , and references therein). This outflow is easily identified in the H $\alpha$ + [N II] flux intensity contours included in the top-left panel of Fig. 4, having the archetypical biconical shape. The origin of this galactic outflow is under discussion. Based on pure optical spectroscopic data, following the criteria defined by Sharp & Bland-Hawthorn (2010), López-Cobá et al. (2019) determined that this outflows is most probably driven by a strong nuclear SF process. However, it known that this object host an obscured AGN (Ricci et al. 2016), that has been uncovered using

<sup>3</sup> [http://ifs.astroscu.unam.mx/CALIFA/V500/v2.3/new\\_diag/](http://ifs.astroscu.unam.mx/CALIFA/V500/v2.3/new_diag/)

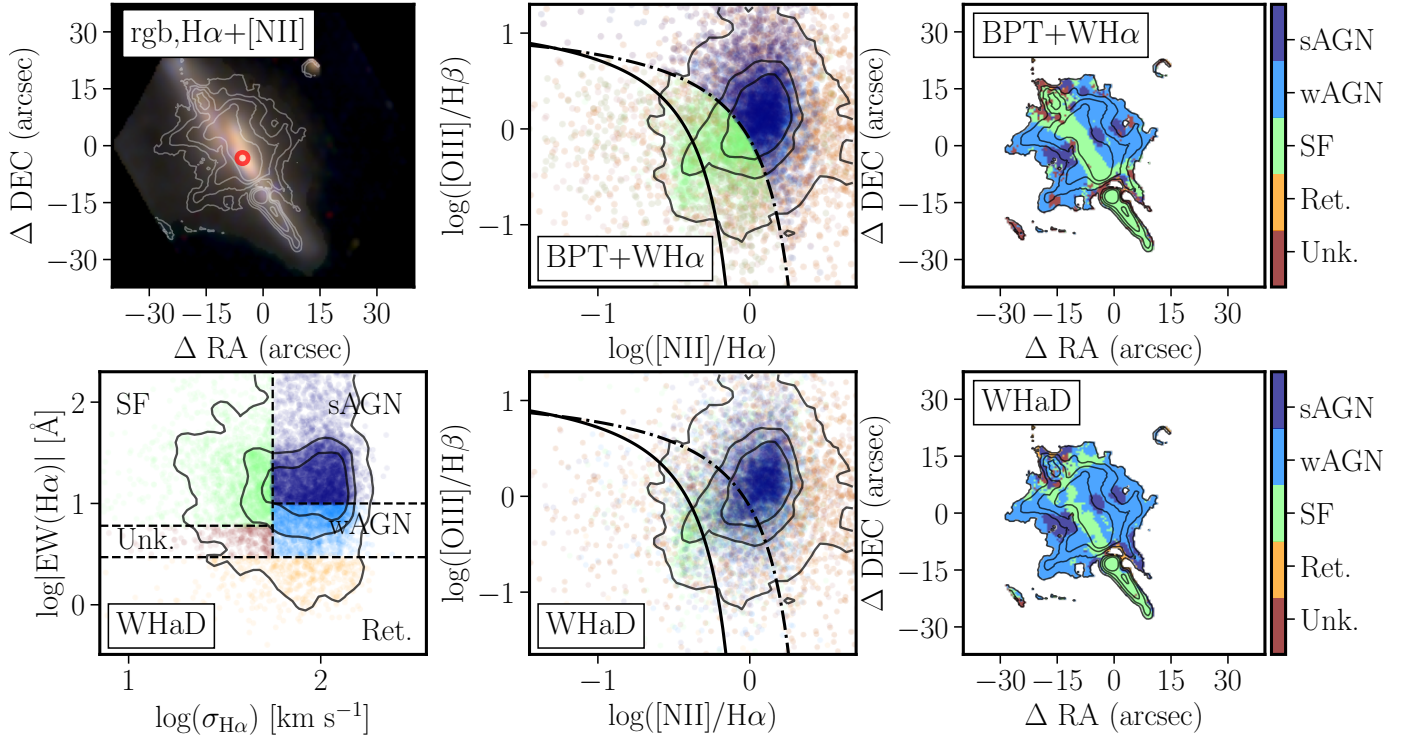


**Fig. 4.** Similar to Fig. 2, corresponding to the eCALIFA data of NGC 6286.

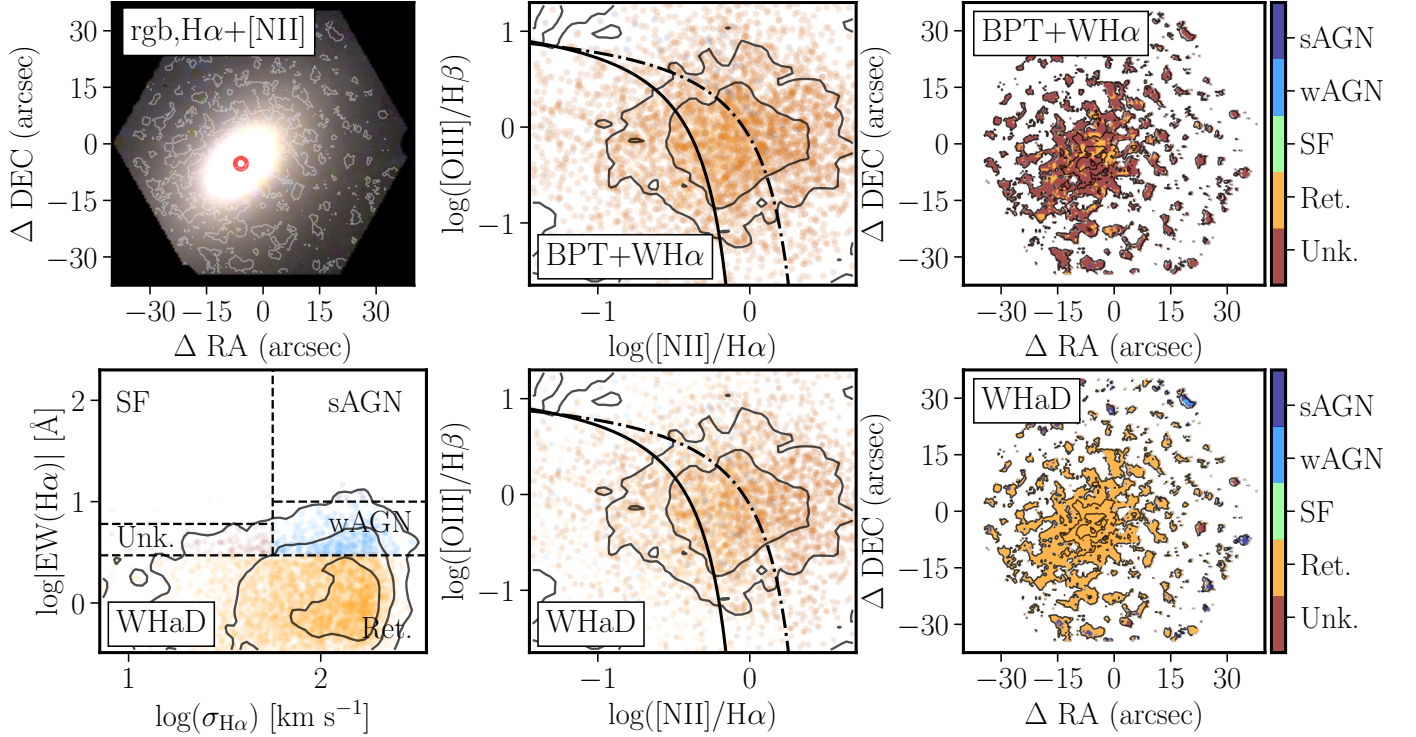


**Fig. 5.** Similar to Fig. 2, corresponding to the eCALIFA data of NGC 3610

X-ray observations. Irrespectively of the physical origin of the galactic wind that generated the outflow, the gas along its biconical structure is clearly ionized by shocks. This is appreciated in top-central and top-right panels of Fig. 4: using the BPT+WHα criteria the ionized gas at the location of the outflows is classified as wAGN/sAGN. Note, once again that this is what it is expected for a shock-ionized gas. In addition, the gas along the edge-on disk is mostly ionized by a SF process. When applying

the new classification scheme (bottom panels), we find a very similar result, with subtle differences (for instance, the width of the regime classified as SF along the edge-on disk is slightly narrower when using the new scheme). We performed a visual inspection of all the galaxies with detected outflows within the CALIFA sample (López-Cobá et al. 2019), finding similar consistent results. In summary, using the WHaD diagram it is feasi-

ble to identify shock-ionized galactic outflows as well as using the BPT+WHa scheme.

Finally, Figure 5 is similar to Fig. 2-4, for an archetypical retired galaxy, NGC 3610. This is an intermediate mass ( $M_{\star} \sim 10^{10.3} M_{\odot}$ ) elliptical galaxy, with a weak/diffuse ionized gas emission distributed across most of the FoV of the IFU data (top-left panel of Fig. 5). It presents a weak and soft X-ray emission that is not compatible with the presence of an AGN (Fabiano & Schweizer 1995). Despite of the nature of this object (a true elliptical galaxy or an early-spiral with a very low dist-to-bulge ratio), its ionized gas is clearly classified as retired using the BPT+WHa (top-central and top-right panels of Fig. 5). Note that a substantial fraction of the spaxels with detected ionized gas would be classified as unknown if a cut in the S/N ratio of all the lines involved in the BPT diagram is considered. Using just the EW( $H\alpha$ ) they would be classified as retired, being most probably ionized by hot evolved low mass stars in the post-AGB phases. By construction the WHaD diagram performs a similar classification, being the difference that most of the regions which ionizing source is labelled as unknown when using the full dataset required to explore the BPT diagram are known directly classified as retired.

In summary we have illustrated how the use of the WHaD classification scheme, based on one single emission line, provides a reliable classification of ionizing source for the spatial resolved ionized gas in galaxies. This classification is compatible, in general, with the one provided by the BPT+WHa scheme. The reported differences may reflect possible misclassification cases (e.g., central AGN in NGC 5947) or the uncover of previously undetected/missed ionizing sources (e.g., central AGN in NGC 5947 again, and the SNR in NGC 2906).

#### 4. Conclusions

We motivate this work discussing the problems to identify the ionizing source in galaxies based on the most commonly used method. This method uses the O3 vs. N2 BPT diagram, identifying regions in which different ionizing sources are dominant or more frequently observed. The method present intrinsic problems, due to (i) the S/N requirements and the wide range of relative fluxes between the involved emission lines, and (ii) the confusion among regimes in which different ionizing source could reproduce the observed line ratios. While the later problem has been addressed in the literature by the inclusion of additional parameters, such as the EW( $H\alpha$ ) and/or  $\sigma_{\text{vel}}$ , to overcome these problems, the former one cannot be so easily addressed.

We have proposed an new method that explores the location of different ionizing sources in a new diagram (WHaD), that compares EW( $H\alpha$ ) and  $\sigma_{\text{vel}}$ . This diagram has the virtue of using just one single emission line, typically the strongest one in the optical range for all ionizing sources. We use IFU data from eCALIFA and MaNGA in combination with literature data, to explore the location of different ionizing sources classified using the standard procedure (BPT+WHa method) and bona-fide X-ray selected AGNs. Based on that exploration we define different areas in which the ionizing source could be classified as: (i) SF, ionization due to young-massive OB stars, related to recent star-formation activity; (ii) sAGNs/wAGNs, ionization due to strong (weak) AGNs, and other sources of ionizations like high velocity shocks; and (iii) RG, ionization due to hot old low-mass evolved stars (post-AGBs), associated with retired galaxies and regiones within galaxies (regions in which there is no star-formation).

We applied the new classification to (i) the same dataset adopted to define the method and to (ii) the full dataset of spatial

resolved spectroscopic data provided by the eCALIFA survey, comparing the results provided by the two methods (BPT+WHa vs. WHaD). We found that:

1. Both methods provides exactly the same classification for retired regions and galaxies, when only EW( $H\alpha$ ) is considered. If the full set of emission lines required to explore the BPT diagram is used the new method recovers a larger number of galaxies/regions that cannot be classified using the BPT+WHa method.
2. 90% (86-95%) of the galaxies classified as SF (O-AGNs) using the BPT+WHa method would be equally classified using the WHaD diagram.
3. Around 99% (50-73%) of the galaxies classified as SF (O-AGNs) using the WHaD diagram were equally classified using the BPT+WHa method.
4. Around 50% of the X-AGNs have been classified as O-AGNs using the WHaD method, a significantly larger fraction than the number than the one recovered using the more traditional BPT+WHa diagram (17-34%).
5. The spatial resolved classification provided by the WHaD is similar to the one provided by the BPT+WHa one for star-forming, retired and high-speed shock ionized regions. However, it increases the number of AGN candidates and AGN-like ionizing sources, that in addition have a more realistic distribution in the BPT diagram that the one shown by O-AGNs.

In summary we consider that the proposed method is an useful tool when all the set of emission lines required for other diagnostic diagrams are not accesible due to the wavelength range covered by the observations (e.g., in Fabry-Perot observations in many cases) or some of them lack sufficient signal-to-noise for a proper exploration (e.g., in the case of  $H\beta$  for dusty galaxies or regions within galaxies). The method has been proved for low- $z$  ( $z \sim 0.01$ ) integrated and spatially resolved data. Any attempt to apply it at higher redshifts would require a re-evaluation of the method and the proposed boundaries, which is beyond the scope of the current exploration.

*Acknowledgements.* We thanks the anonymous referee for the comments that have improved this manuscript. S.F.S. thanks the PAPIIT-DGAPA AG100622 project. J.K.B.B. and S.F.S. acknowledge support from the CONACYT grant CF19-39578. JSA acknowledges financial support from the Spanish Ministry of Science and Innovation (MICINN), project PID2019-107408GB-C43 (ESTALLIDOS). Integral Field Area (CALIFA) survey (<http://califa.caha.es/>), observed at the Calar Alto Observatory. Based on observations collected at the Centro Astronómico Hispano Alemán (CAHA) at Calar Alto, operated jointly by the Max-Planck-Institut für Astronomie and the Instituto de Astrofísica de Andalucía (CSIC). This project makes use of the MaNGA-Pipe3D dataproducts. We thank the IA-UNAM MaNGA team for creating this catalogue, and the Conacyt Project CB-285080 for supporting them. This research made use of Astropy,<sup>4</sup> a community-developed core Python package for Astronomy (Astropy Collaboration et al. 2013, 2018). Funding for the Sloan Digital Sky Survey IV has been provided by the Alfred P. Sloan Foundation, the U.S. Department of Energy Office of Science, and the Participating Institutions. SDSS-IV acknowledges support and resources from the Center for High Performance Computing at the University of Utah. The SDSS website is [www.sdss.org](http://www.sdss.org). SDSS-IV is managed by the Astrophysical Research Consortium for the Participating Institutions of the SDSS Collaboration including the Brazilian Participation Group, the Carnegie Institution for Science, Carnegie Mellon University, Center for Astrophysics | Harvard & Smithsonian, the Chilean Participation Group, the French Participation Group, Instituto de Astrofísica de Canarias, The Johns Hopkins University, Kavli Institute for the Physics and Mathematics of the Universe (IPMU) / University of Tokyo, the Korean Participation Group, Lawrence Berkeley National Laboratory, Leibniz Institut für Astrophysik Potsdam (AIP), Max-Planck-Institut für Astronomie (MPIA Heidelberg), Max-Planck-Institut für Astrophysik (MPA Garching), Max-Planck-Institut für Extraterrestrische Physik (MPE), National Astronomical Observatories of China, New Mexico State University, New York

<sup>4</sup> <http://www.astropy.org>

University, University of Notre Dame, Observatório Nacional / MCTI, The Ohio State University, Pennsylvania State University, Shanghai Astronomical Observatory, United Kingdom Participation Group, Universidad Nacional Autónoma de México, University of Arizona, University of Colorado Boulder, University of Oxford, University of Portsmouth, University of Utah, University of Virginia, University of Washington, University of Wisconsin, Vanderbilt University, and Yale University.

## References

- Abdurro'uf, Accetta, K., Aerts, C., et al. 2021, arXiv e-prints, arXiv:2112.02026
- Agostino, C. J. & Salim, S. 2019, *ApJ*, 876, 12
- Agostino, C. J., Salim, S., Ellison, S. L., Bickley, R. W., & Faber, S. M. 2023, *ApJ*, 943, 174
- Agostino, C. J., Salim, S., Faber, S. M., et al. 2021, *ApJ*, 922, 156
- Albán, M. & Wylezalek, D. 2023, arXiv e-prints, arXiv:2302.08519
- Astropy Collaboration, Price-Whelan, A. M., SipHocz, B. M., et al. 2018, *aj*, 156, 123
- Astropy Collaboration, Robitaille, T. P., Tollerud, E. J., et al. 2013, *A&A*, 558, A33
- Bacon, R., Accardo, M., Adjali, L., et al. 2010, in *SPIE Conf. Series*, Vol. 7735
- Baldwin, J. A., Phillips, M. M., & Terlevich, R. 1981, *PASP*, 93, 5
- Barrera-Ballesteros, J. K., Heckman, T., Sánchez, S. F., et al. 2018, *ApJ*, 852, 74
- Belfiore, F., Maiolino, R., Maraston, C., et al. 2017, *MNRAS*, 466, 2570
- Binette, L., Magris, C. G., Stasińska, G., & Bruzual, A. G. 1994, *A&A*, 292, 13
- Bluck, A. F. L., Maiolino, R., Sanchez, S., et al. 2019, arXiv e-prints, arXiv:1911.08857
- Bundy, K., Bershady, M. A., Law, D. R., et al. 2015, *ApJ*, 798, 7
- Cano-Díaz, M., Sánchez, S. F., Zibetti, S., et al. 2016, *ApJ*, 821, L26
- Cid Fernandes, R., Carvalho, M. S., Sánchez, S. F., de Amorim, A., & Ruschel-Dutra, D. 2021, *MNRAS*, 502, 1386
- Cid Fernandes, R., Stasińska, G., Schlickmann, M. S., et al. 2010, *MNRAS*, 403, 1036
- Comerford, J. M., Negus, J., Müller-Sánchez, F., et al. 2020, *ApJ*, 901, 159
- D'Agostino, J. J., Kewley, L. J., Groves, B. A., et al. 2019, *MNRAS*, 487, 4153
- Davies, R. L., Groves, B., Kewley, L. J., et al. 2016, *MNRAS*, 462, 1616
- Dopita, M. A., Koratkar, A. P., Evans, I. N., et al. 1996, in *Astronomical Society of the Pacific Conference Series*, Vol. 103, *The Physics of Liners in View of Recent Observations*, ed. M. Eracleous, A. Koratkar, C. Leitherer, & L. Ho, 44
- Driver, S. P., Norberg, P., Baldry, I. K., et al. 2009, *Astronomy and Geophysics*, 50, 5.12
- Espinosa-Ponce, C., Sánchez, S. F., Morisset, C., et al. 2020, *MNRAS*, 494, 1622
- Fabbiano, G. & Schweizer, F. 1995, *ApJ*, 447, 572
- Gil de Paz, A., Carrasco, E., Gallego, J., et al. 2018, in *Society of Photo-Optical Instrumentation Engineers (SPIE) Conference Series*, Vol. 10702, *Ground-based and Airborne Instrumentation for Astronomy VII*, ed. C. J. Evans, L. Simard, & H. Takami, 1070217
- Guidi, G., Casado, J., Ascasibar, Y., et al. 2018, *MNRAS*, 479, 917
- Heckman, T. M. 1987, in *Observational Evidence of Activity in Galaxies*, ed. E. E. Khachikian, K. J. Fricke, & J. Melnick, Vol. 121, 421
- Howell, J. H., Armus, L., Mazzarella, J. M., et al. 2010, *ApJ*, 715, 572
- Ibarra-Medel, H. J., Avila-Reese, V., Sánchez, S. F., González-Samaniego, A., & Rodríguez-Puebla, A. 2019, *MNRAS*, 483, 4525
- Ibarra-Medel, H. J., Sánchez, S. F., Avila-Reese, V., et al. 2016, *MNRAS*, 463, 2799
- Jarvis, B. J. 1990, *Astronomy and Astrophysics*, 240, L8
- Johnston, V. 2022, in *American Astronomical Society Meeting Abstracts*, Vol. 54, *American Astronomical Society Meeting #240*, 230.01
- Johnston, V., Medling, A., Groves, B., et al. 2023, arXiv e-prints, arXiv:2307.11831
- Kauffmann, G., Heckman, T. M., Tremonti, C., et al. 2003, *MNRAS*, 346, 1055
- Kewley, L. J., Dopita, M. A., Sutherland, R. S., Heisler, C. A., & Trevena, J. 2001, *ApJ*, 556, 121
- Kewley, L. J., Nicholls, D. C., & Sutherland, R. S. 2019, *ARA&A*, 57, 511
- Lacerda, E. A. D., Cid Fernandes, R., Couto, G. S., et al. 2018, *MNRAS*, 474, 3727
- Lacerda, E. A. D., Sánchez, S. F., Mejía-Narváez, A., et al. 2022, arXiv e-prints, arXiv:2202.08027
- Law, D. R., Belfiore, F., Bershady, M. A., et al. 2021, arXiv e-prints, arXiv:2112.11281
- Lee, E., Li, W., Boles, T., et al. 2005, *IAU Circ.*, 8628, 1
- López-Cobá, C., Sánchez, S. F., Anderson, J. P., et al. 2020, arXiv e-prints, arXiv:2002.09328
- López-Cobá, C., Sánchez, S. F., Bland-Hawthorn, J., et al. 2019, *MNRAS*, 482, 4032
- López-Cobá, C., Sánchez, S. F., Cruz-González, I., et al. 2017, *ApJ*, 850, L17
- Mejía-Narváez, A., Sánchez, S. F., Carigi, L., et al. 2022, *A&A*, 661, L5
- Osorio-Clavijo, N., González-Martín, O., Sánchez-Sánchez, S. F., Guainazzi, M., & Cruz-González, I. 2023, arXiv e-prints, arXiv:2303.18245
- Osterbrock, D. E. 1989, *Astrophysics of gaseous nebulae and active galactic nuclei* (University Science Books)
- Ricci, C., Bauer, F. E., Treister, E., et al. 2016, *ApJ*, 819, 4
- Sánchez, S. F. 2020, *ARA&A*, 58, 99
- Sánchez, S. F., Avila-Reese, V., Hernandez-Toledo, H., et al. 2018, *Rev. Mexicana Astron. Astrofis.*, 54, 217
- Sánchez, S. F., Avila-Reese, V., Rodríguez-Puebla, A., et al. 2019a, *MNRAS*, 482, 1557
- Sánchez, S. F., Barrera-Ballesteros, J. K., Galbany, L., et al. 2023, arXiv e-prints, arXiv:2304.13070
- Sánchez, S. F., Barrera-Ballesteros, J. K., Lacerda, E., et al. 2022, *ApJS*, 262, 36
- Sánchez, S. F., Barrera-Ballesteros, J. K., López-Cobá, C., et al. 2019b, *MNRAS*, 484, 3042
- Sanchez, S. F., Galbany, L., Walcher, C. J., Garcia-Benito, R., & Barrera-Ballesteros, J. K. 2023, arXiv e-prints, arXiv:2304.13022
- Sánchez, S. F., García-Benito, R., Zibetti, S., et al. 2016a, *A&A*, 594, A36
- Sánchez, S. F., Kennicutt, R. C., Gil de Paz, A., et al. 2012, *A&A*, 538, A8
- Sánchez, S. F., Pérez, E., Sánchez-Blázquez, P., et al. 2016b, *Rev. Mexicana Astron. Astrofis.*, 52, 171
- Sánchez, S. F., Rosales-Ortega, F. F., Iglesias-Páramo, J., et al. 2014, *A&A*, 563, A49
- Sánchez, S. F., Walcher, C. J., Lopez-Cobá, C., et al. 2021a, *Rev. Mexicana Astron. Astrofis.*, 57, 3
- Sánchez, S. F., Walcher, C. J., Lopez-Cobá, C., et al. 2021b, *Rev. Mexicana Astron. Astrofis.*, 57, 3
- Sánchez-Menguiano, L., Sánchez, S. F., Pérez, I., et al. 2018, *A&A*, 609, A119
- Sánchez-Menguiano, L., Sánchez Almeida, J., Muñoz-Tuñón, C., et al. 2019, *ApJ*, 882, 9
- Sarmiento, R., Huertas-Company, M., Knapen, J. H., et al. 2022, arXiv e-prints, arXiv:2211.11790
- Sharp, R. G. & Bland-Hawthorn, J. 2010, *ApJ*, 711, 818
- Singh, R., van de Ven, G., Jahnke, K., et al. 2013, *A&A*, 558, A43
- Stasińska, G., Vale Asari, N., Cid Fernandes, R., et al. 2008, *MNRAS*, 391, L29
- Veilleux, S., Shopbell, P. L., & Miller, S. T. 2001, *AJ*, 121, 198
- York, D. G., Adelman, J., Anderson, Jr., J. E., et al. 2000, *AJ*, 120, 1579